Dual frequency open-loop electric potential microscopy for local potential measurements in electrolyte solution with high ionic strength

doi: 10.1063/1.3698207

AIP | Review of Scientific Instruments

Dual frequency open-loop electric potential microscopy for local potential measurements in electrolyte solution with high ionic strength

Naritaka Kobayashi, Hitoshi Asakawa, and Takeshi Fukuma

Citation: Rev. Sci. Instrum. **83**, 033709 (2012); doi: 10.1063/1.3698207
View online: http://dx.doi.org/10.1063/1.3698207
View Table of Contents: http://rsi.aip.org/resource/1/RSINAK/v83/i3
Published by the American Institute of Physics.

Dual frequency open-loop electric potential microscopy for local potential measurements in electrolyte solution with high ionic strength

Naritaka Kobayashi,[1] Hitoshi Asakawa,[2] and Takeshi Fukuma[1,2,a)]
[1]*Frontier Science Organization, Kanazawa University, Kakuma-machi, Kanazawa 920-1192, Japan*
[2]*Bio-AFM Frontier Research Center, Kanazawa University, Kakuma-machi, Kanazawa 920-1192, Japan*

(Received 13 January 2012; accepted 10 March 2012; published online 30 March 2012)

Recent development of open-loop electric potential microscopy (OL-EPM) has enabled to measure local potential distribution at a solid/liquid interface. However, the operating environment of OL-EPM has been limited to a weak electrolyte solution (<1 mM). This has significantly limited its application range in biology and chemistry. To overcome this limitation, we have developed dual frequency (DF) mode OL-EPM. In the method, an ac bias voltage consisting of two frequency components at f_1 and f_2 is applied between a tip and sample. The local potential is calculated from the amplitudes of the f_1 and $|f_1 - f_2|$ components of the electrostatic force. In contrast to the conventional single frequency (SF) mode OL-EPM, the detection of the $2f_1$ component is not required in DF mode. Thus, the maximum bias modulation frequency in DF mode is twice as high as that in SF mode. The high bias modulation frequency used in DF mode prevents the generation of electrochemical reactions and redistribution of ions and water, which enables to operate OL-EPM even in a strong electrolyte solution. In this study, we have performed potential measurements of nanoparticles on a graphite surface in 1 and 10 mM NaCl solution. The results demonstrate that DF mode OL-EPM allows measurements of local potential distribution in 10 mM electrolyte solution. © *2012 American Institute of Physics*. [http://dx.doi.org/10.1063/1.3698207]

I. INTRODUCTION

Local potential distribution at a solid/liquid interface plays important roles in various processes in biological systems and industrial devices (e.g., battery and catalyst). To understand the mechanism of these processes, it is desirable to directly measure the local potential distribution in liquid with nanoscale resolution. To date, potential measurements in liquid have mainly been performed using electrophoresis.[1] However, this method gives a zeta potential averaged over the sample surface and does not allow us to measure local potential distribution. Another approach is force curve measurements by atomic force microscopy (AFM) using a colloidal probe[2] or a blunt tip.[3] However, the spatial resolution of this approach has been limited to ≈100 nm. Therefore, it has been difficult to discuss the relationship between local potential distribution and the biological and chemical processes at a solid/liquid interface.

Kelvin probe force microscopy (KFM) (Refs. 4 and 5) is one of the surface property measurement techniques based on AFM. The method allows simultaneous measurements of surface topography and local potential distribution on various materials such as semiconducting,[6] organic,[7] and biological[8] materials. However, the operating environment of KFM has been limited to ambient and vacuum conditions. KFM cannot be operated in liquid unless inert organic solvent is used. If we operate KFM in electrolyte solution, ac and dc bias voltages applied between a tip and sample cause unwanted electrochemical reactions and redistribution of ions and water. These events vary surface energy of a cantilever and sample, generating uncontrollable spurious force (F_{sp}). This force prevents stable operation of KFM. In addition, these events often modify surface structures and properties of a sample. Thus, the reliability and reproducibility of the measurements cannot be secured.

Recently, we have overcome these difficulties by developing open-loop electric potential microscopy (OL-EPM).[9] In OL-EPM, only an ac bias voltage with a relatively high modulation frequency (f_m > 30 kHz) is applied between a tip and sample. This prevents electrochemical reactions and redistribution of ions and water. Hence, the generation of F_{sp} is greatly suppressed. The application of an ac bias voltage induces tip-sample electrostatic force (F_{es}). The potential value (V_s) at the proximity of the sample surface is calculated from the first and second harmonic oscillation amplitudes (A_1 and A_2, respectively) of a cantilever induced by F_{es}. In the previous study, we demonstrated that OL-EPM allows quantitative measurements of local potential distribution in electrolyte solution with nanoscale spatial and millivolt potential resolutions.[9,10]

So far, OL-EPM has been used only in a relatively weak electrolyte solution (1 mM NaCl solution). However, the ionic strength of the solution used in practical applications in biology and electrochemistry is often much higher than that. The electrochemical reactions and redistribution of ions and water are induced by F_{es} at a frequency lower than a threshold value (f_c). Thus, the suppression of F_{sp} in a strong electrolyte solution requires high f_m. However, if f_m is too high, $2f_m$ can exceed the cantilever resonance frequency (f_0) and the detection sensitivity of A_2 is deteriorated. One of the solutions to this problem is to use a high-f_0 cantilever. However, at present, f_0 of a commercially available cantilever is less than 800 kHz in liquid. Thus, f_m should be sufficiently

a)Electronic mail: fukuma@staff.kanazawa-u.ac.jp.

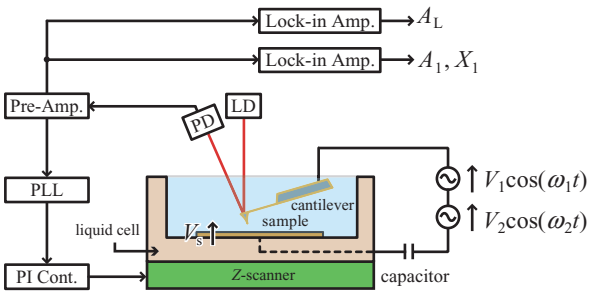

FIG. 1. Schematic drawing of the experimental setup for DF mode OL-EPM in liquid. A capacitor is inserted into the bias circuit to prevent an accidental application of a dc bias voltage. The cantilever oscillation was excited by the photothermal excitation method, which is not shown here for clarity.

lower than 400 kHz. Consequently, the operating environment of OL-EPM has been limited to a weak electrolyte solution (∼1 mM), which has prevented practical applications of OL-EPM in biology and electrochemistry.

In this study, we have developed an improved operation mode of OL-EPM for the measurements in strong electrolyte solution. Here we present the basic principle of the improved operation mode. We have performed potential measurements of nanoparticles in 1 and 10 mM NaCl solutions. By comparing the results obtained by the improved and conventional methods, we discuss the quantitative capability of the developed method and its applicability to a strong electrolyte solution.

II. BASIC PRINCIPLE

Recently, various AFM methods using multiple frequency responses of a cantilever have been proposed such as intermodulation AFM (Ref. 11) and bimodal AFM.[12] Similarly, we also used dual frequency responses of a cantilever in the improved OL-EPM. Namely, an ac bias voltage consisting of two frequency components at $f_1(=\omega_1/2\pi)$ and $f_2(=\omega_2/2\pi)$ is applied between a tip and sample (Fig. 1). The tip-sample potential difference (V_{ts}) is given by

$$V_{ts} = V_1\cos(\omega_1 t) + V_2\cos(\omega_2 t) - V_s, \tag{1}$$

where V_1 and V_2 are the amplitudes of the f_1 and f_2 components of the ac bias voltage, respectively.

F_{es} induced by the ac bias voltage is given by

$$\begin{aligned} F_{es} &= \frac{1}{2}\frac{\partial C_{ts}}{\partial z}V_{ts}^2 \\ &= \frac{1}{2}\frac{\partial C_{ts}}{\partial z}\left[\left(V_s^2 + \frac{1}{2}V_1^2 + \frac{1}{2}V_2^2\right)\right. \\ &\quad -2V_s\{V_1\cos(\omega_1 t) + V_2\cos(\omega_2 t)\} \\ &\quad +\frac{1}{2}\left\{V_1^2\cos(2\omega_1 t) + V_2^2\cos(2\omega_2 t)\right\} \\ &\quad \left.+V_1V_2\{\cos(\omega_H t) + \cos(\omega_L t)\}\right], \end{aligned} \tag{2}$$

where C_{ts} and z are tip-sample capacitance and Z position of a tip, respectively. ω_H and ω_L are defined by following equations.

$$\omega_H = \omega_1 + \omega_2. \tag{3}$$

$$\omega_L = \omega_1 - \omega_2. \tag{4}$$

In this method, we use $f_L(=\omega_L/2\pi)$ component instead of $2f_1$ component used in the conventional method. f_L component can be detected with sufficient sensitivity by setting f_1 and f_2 to satisfy $f_L < f_0$.

From Eq. (2), amplitudes of cantilever oscillation at f_1 and f_L (A_1 and A_L, respectively) are given by

$$A_1 = G(\omega_1)\left|\frac{\partial C_{ts}}{\partial z}V_s\right|V_1, \tag{5}$$

$$A_L = G(\omega_L)\left|\frac{\partial C_{ts}}{\partial z}\right|\frac{V_1V_2}{2}, \tag{6}$$

where $G(\omega)$ is the transfer function of a cantilever. $G(\omega)$ is given by

$$G(\omega) = \frac{1}{k}\frac{1}{\sqrt{[1-(\omega/\omega_0)^2]^2 + [\omega/(Q\omega_0)]^2}}, \tag{7}$$

where Q is Q-factor of a cantilever.

From Eqs. (5) and (6), $|V_s|$ is obtained as

$$|V_s| = \frac{V_2}{2}\frac{A_1}{A_L}\frac{G(\omega_L)}{G(\omega_1)}. \tag{8}$$

The polarity of V_s can be determined in the same way as in the conventional OL-EPM from the phase difference (ϕ_1) between the cantilever oscillation and f_1 component of the ac bias voltage. Therefore, V_s is given by

$$\begin{aligned} V_s &= \mathrm{sgn}(\cos\phi_1)\frac{V_2}{2}\frac{A_1}{A_L}\frac{G(\omega_L)}{G(\omega_1)}, \\ &= \mathrm{sgn}(X_1)\frac{V_2}{2}\frac{A_1}{A_L}\frac{G(\omega_L)}{G(\omega_1)}, \end{aligned} \tag{9}$$

where X_1 is defined as $X_1 \equiv A_1\cos\phi_1$.

In the improved method, the detection of A_2 is not required. Thus, the maximum bias modulation frequency in the improved method is twice as high as that in the conventional OL-EPM. The high bias modulation frequency prevents the generation of electrochemical reactions and redistribution of ions and water, which enables to operate OL-EPM even in a strong electrolyte solution. We hereafter refer to the conventional and improved methods as single frequency (SF) and dual frequency (DF) mode OL-EPM, respectively.

III. EXPERIMENTAL DETAILS

Figure 1 shows the experimental setup of DF mode OL-EPM used in this study. A home-built AFM with a low noise optical beam deflection sensor[13–15] was used. DF mode OL-EPM can be combined with any AFM operation modes including amplitude,[16] frequency,[17] and phase[18] modulation AFM (AM-, FM-, or PM-AFM). In this study, we combined it with FM-AFM. In FM-AFM, a cantilever is oscillated at f_0 with constant oscillation amplitude (A) using a phase-locked

loop (PLL) circuit (OC4: SPECS). The tip-sample distance is regulated by keeping the frequency shift (Δf) constant. Δf is detected with the PLL circuit. The feedback control and image acquisition were performed by a commercially available AFM controller (RC4: SPECS).

Si cantilevers (AC55: Olympus) with k and f_0 of ~85 N/m and ~700 kHz in liquid, respectively, were used in this experiment. The cantilevers were supplied with a gold backside coating (thickness: 50 nm). In addition, we coated the front side of the cantilever with a gold thin film by sputtering method (thickness: 50 nm). The cantilever was oscillated by the photothermal excitation method.[15,19]

An ac bias voltage was produced by adding a sine wave $V_2\cos(\omega_2 t)$ from a function generator (AFG3022B: Tektronix) to another sine wave $V_1\cos(\omega_1 t)$ from a lock-in amplifier (HF2LI: Zurich Instruments). The bias voltage was applied between a tip and sample. A_1, A_2, and X_1 were derived from the cantilever deflection signal with the lock-in amplifier.

The sample used for the potential measurements was prepared as follows. The stock solution of the latex beads (01-02-251: Micromod) was diluted with pure water to 100 μg/ml. The beads have a nominal diameter of 25 nm. The surface of the beads is terminated with amino groups. The solution was sonicated for 30 min to disperse the aggregated latex beads. The solution was dropped onto the cleaved surface of a highly oriented pyrolytic graphite (HOPG) (ZYA: NT-MDT) substrate. The sample was left for 5 min and the remaining solution was removed by N_2 blow. The potential measurement was performed in 1 or 10 mM NaCl solution.

IV. RESULTS AND DISCUSSION

A. Dependence of f_c on ionic strength

Figures 2(a) and 2(b) show A_1 versus frequency curves measured in 1 and 10 mM NaCl solutions, respectively. The A_1 curves show a peak at f_0 due to the influence of $G(\omega)$. We have eliminated this influence as follows. We estimated f_0 and Q by fitting the thermal vibration spectrum of the cantilever to Eq. (7). The normalized transfer function $[\hat{G}(\omega)(\equiv kG(\omega))]$ of a cantilever was calculated from the estimated values of f_0 and Q. We divided A_1 by $\hat{G}(\omega)$ to obtain $\hat{A}_1(= A_1/\hat{G}(\omega))$. This value is proportional to the force acting on the cantilever and free of the influence from $G(\omega)$.

The $\hat{A}_1$ curves show an increase at the low frequency range due to the influence of F_{sp}.[20] This influence extends up to a certain threshold frequency f_c. Above f_c, $\hat{A}_1$ shows an approximately constant value ($\hat{A}_1^0$). If we define f_c as a frequency where the deviation of $\hat{A}_1$ from $\hat{A}_1^0$ exceeds 10%, it corresponds to 50 and 300 kHz in 1 and 10 mM NaCl solutions, respectively. The result shows that f_c significantly increases with increasing the ionic strength. This is because the time response of the electrochemical reactions and redistribution of ions and water should be enhanced by the increase of ionic strength. These results show that the bias modulation frequency should be sufficiently higher than 50 and 300 kHz in 1 and 10 mM electrolyte solutions, respectively.

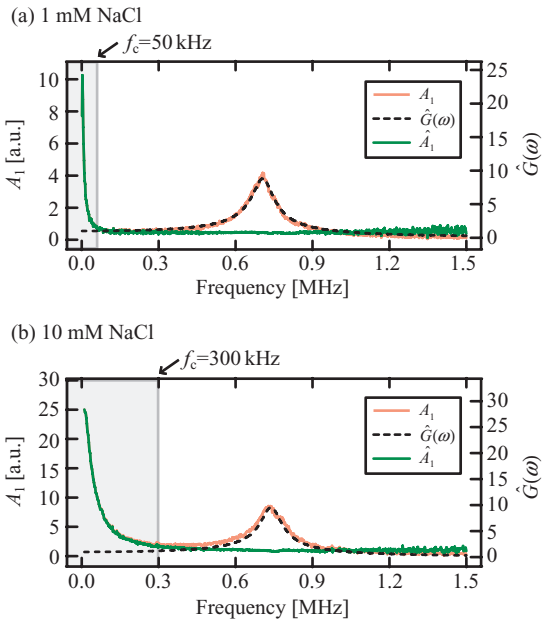

FIG. 2. Frequency dependence of A_1, $\hat{G}(\omega)$, and $\hat{A}_1$ measured in NaCl solution. (a) 1 mM, $f_0 = 708.3$ kHz, $Q = 8.8$. (b) 10 mM, $f_0 = 740.6$ kHz, $Q = 9.6$. f_0 and Q were estimated by fitting the thermal vibration spectrum of the cantilever to Eq. (7). $\hat{G}(\omega)$ was calculated from the estimated values of f_0 and Q. $\hat{A}_1$ was obtained by dividing A_1 by $\hat{G}(\omega)$.

B. Potential measurements in 1 mM NaCl solution

In the previous study, we demonstrated the quantitative capability of SF mode OL-EPM by comparing the potential of nanoparticles measured by OL-EPM and that measured by electrophoresis in 1 mM NaCl solution.[10] In this study, we have performed potential measurements by SF and DF modes under the same experimental condition (Fig. 3). Thus, we can confirm the basic principle of DF mode by comparing the results obtained by the two methods.

1. Detection of electrostatic force

As discussed in Sec. IV A [Fig. 2(a)], the bias modulation frequencies (f_1 and f_2) should be higher than 50 kHz to avoid the generation of F_{sp} in 1 mM NaCl solution. In addition, these frequencies should be lower than $f_0(= 708$ kHz) to obtain sufficient sensitivity of the A_1 detection. In this experiment, we set f_1 and f_2 at 600 and 630 kHz, respectively.

Figure 3(a) shows a voltage spectral density distribution of the cantilever deflection signal measured in 1 mM NaCl solution. During the measurement, the tip-sample distance was regulated to keep Δf at +500 Hz. The sharp decrease observed at the frequency below 10 kHz is caused by a low-pass filter at the input of the FFT analyzer. Several peaks are found in the spectrum shown in Fig. 3(a). The peak at f_0 corresponds to the cantilever vibration induced by the photothermal excitation while the others correspond to the vibration induced by F_{es}. F_{es} consists of several frequency components as described in Eq. (2). The frequency of each component agrees to the position of the corresponding peak as indicated by arrows in Fig. 3(a).

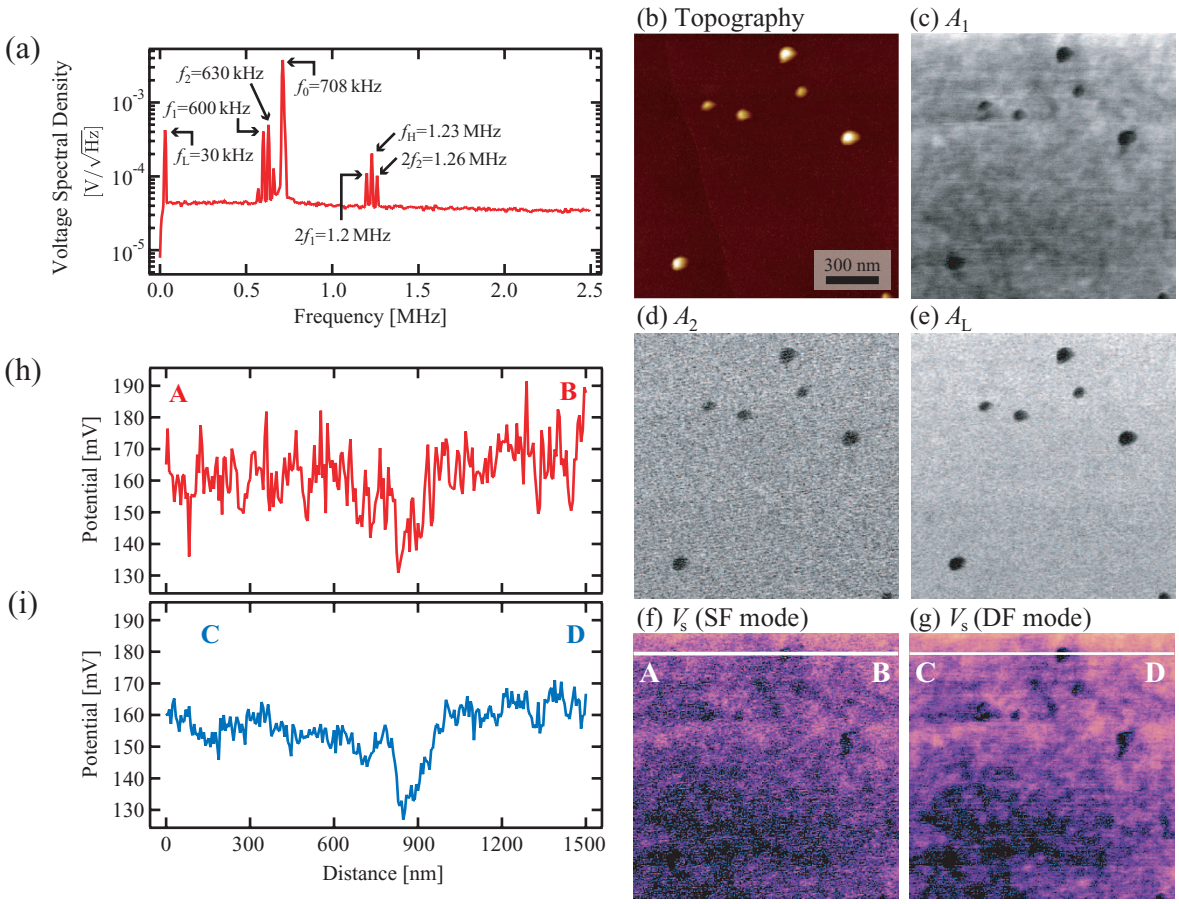

FIG. 3. (a) Voltage spectral density distribution of the cantilever deflection signal measured in 1 mM NaCl solution. (b) Topographic, (c) A_1, (d) A_2, (e) A_L, (f) potential (SF mode), and (g) potential (DF mode) images of nanoparticles on the HOPG surface obtained in 1 mM NaCl solution (scan size: 1.5 μm × 1.5 μm, $f_0 = 708.3$ kHz, $Q = 8.8$, $k = 36.2$ N/m, $A = 0.54$ nm, $\Delta f = -300$ Hz, $f_1 = 600$ kHz, $f_2 = 630$ kHz, $V_1 = V_2 = 1$ V). Potential profiles measured along (h) line A-B in (f) (SF mode) and (i) line C-D in (g) (DF mode).

The magnitude of the f_L component (424 $\mu V/\sqrt{Hz}$) is 3.8 times larger than that of the $2f_1$ component (111 $\mu V/\sqrt{Hz}$). From Eq. (2), the ratio of A_L to A_2 is given by

$$\frac{A_L}{A_2} = \frac{2V_2}{V_1}\frac{G(\omega_L)}{G(2\omega_1)}. \tag{10}$$

The value of A_L/A_2 calculated from this equation is 3.7 [$\hat{G}(\omega_L) = 1.000$, $\hat{G}(2\omega_1) = 0.54$, $V_1 = V_2 = 1$ V], which agrees with the experimentally obtained value. The result shows that the difference between the magnitudes of A_2 and A_L can be explained by the difference between $G(2\omega_1)$ and $G(\omega_L)$. Due to this difference, the detection sensitivity to the f_L component is higher than that to the f_2 component.

2. Potential distribution measurements

Figure 3(b) shows the topographic image of the nanoparticles on the HOPG surface obtained in 1 mM NaCl solution. The image shows several bright spots corresponding to the nanoparticles. Figures 3(c)–3(e) show A_1, A_2, and A_L images simultaneously obtained with the topographic image. From A_1 and A_2 images, we have calculated the potential image in SF mode [Fig. 3(f)]. Similarly, from A_1 and A_L images, we have calculated the potential image in DF mode [Fig. 3(g)].

Figures 3(h) and 3(i) show potential profiles measured along line A-B in Fig. 3(f) and line C-D in Fig. 3(g), respectively. The both profiles show that the potential of the nanoparticles is ~30 mV lower than that of the HOPG substrate. Namely, the potential values measured in DF mode agree with those measured in SF mode. The result confirms the validity of the operation principle of DF mode OL-EPM.

The potential profile measured in SF mode [Fig. 3(h)] shows larger noise than that measured in DF mode [Fig. 3(i)]. This is because the sensitivity to A_2 is much lower than that to A_L due to the influence of $G(\omega)$. This result demonstrates that the use of DF mode improves the potential resolution of OL-EPM when f_1 is set at a relatively high frequency satisfying $2f_1 > f_0$.

3. Dependence on tip-sample distance

Figures 4(a) and 4(b) show the tip-sample distance dependence of A_1, A_2, and A_L. All the signals increase with decreasing the tip-sample distance. While the distance dependence of A_1 reflects the influence of $|\partial C_{ts}/\partial z|$ and $|V_s|$, that

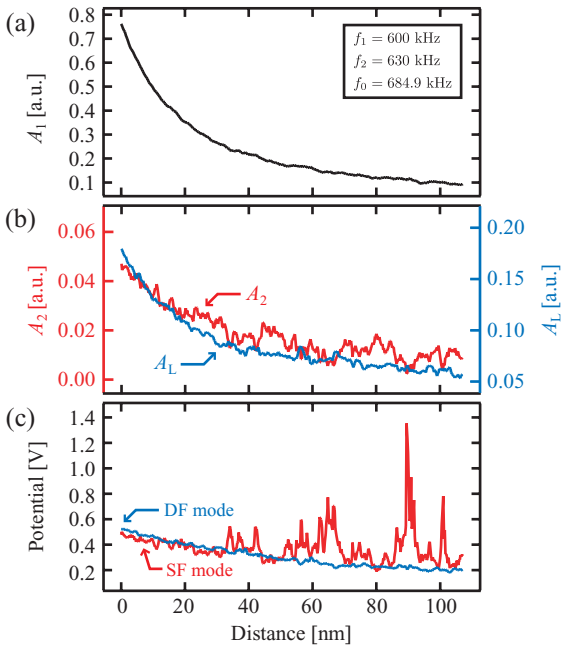

FIG. 4. Dependence on the tip-sample distance measured in 1 mM NaCl solution on the HOPG surface. (a) A_1. (b) A_2 and A_L. (c) Potential calculated in SF and DF modes ($f_0 = 684.9$ kHz, $Q = 11$, $k = 17.9$ N/m, $f_1 = 600$ kHz, $f_2 = 630$ kHz, $V_1 = V_2 = 1$ V).

of A_2 and A_L reflects only the influence of $|\partial C_{ts}/\partial z|$. Thus, the increase of A_2 and A_L can be explained by the increase of $|\partial C_{ts}/\partial z|$ with decreasing the tip-sample separation.

By calculating the ratio of A_1 to A_2 (or A_L), we can eliminate the influence of $|\partial C_{ts}/\partial z|$ and obtain the distance dependence of $|V_s|$ as shown in Fig. 4(c). The result shows that $|V_s|$ values calculated in both SF and DF modes increase with decreasing the tip-sample distance. Therefore, the increase of A_1 observed in Fig. 4(a) is caused by the influence of both $|\partial C_{ts}/\partial z|$ and $|V_s|$.

In Fig. 4(b), the distance dependence of A_L agrees with that of A_2. Furthermore, in Fig. 4(c), potential curve calculated in DF mode quantitatively agrees with that in SF mode. These results suggest that the same physical quantity is measured in both SF and DF modes.

Figure 4(b) shows that noise in the A_2 curve is much larger than that in the A_L curve. As a result, the potential curve calculated from the A_2 curve in SF mode shows larger noise than that calculated from the A_L curve in DF mode [Fig. 4(c)]. These results demonstrate that DF mode enables to measure potential values with higher signal-to-noise ratio (SNR) than SF mode when a relatively high modulation frequency is used. This is consistent with the conclusion obtained in Sec. IV B 2.

C. Measurements in 10 mM NaCl solution

To date, SF mode OL-EPM has been used only in a weak electrolyte solution (<1 mM). Here, we perform potential measurements of nanoparticles in 10 mM NaCl solution to confirm the applicability of DF mode OL-EPM to a strong electrolyte solution.

1. Detection of electrostatic force

From the results shown in Fig. 2(b), the bias modulation frequencies (f_1 and f_2) should be higher than 300 kHz to avoid the generation of F_{sp} in 10 mM NaCl solution. In addition, these frequencies should be lower than f_0(= 740.6 kHz) to obtain sufficient sensitivity of the A_1 detection. In this experiment, we set f_1 and f_2 at 650 kHz and 680 kHz, respectively.

Figure 5(a) shows voltage spectral density distribution of the cantilever deflection signal measured in 10 mM NaCl solution. During the measurement, the tip-sample distance was regulated to keep Δf at +500 Hz. The spectrum shows several peaks. A peak at f_0 corresponds to the cantilever vibration induced by the photothermal excitation while the other peaks should correspond to the vibration induced by the force components of F_{es} described in Eq. (2).

The magnitude of f_L(= 30 kHz) component (277 $\mu V/\sqrt{Hz}$) is 4.0 times larger than that of $2f_1$(= 1.3 MHz) component (70 $\mu V/\sqrt{Hz}$). The ratio of A_L to A_2 calculated from Eq. (10) is 4.2 [$\hat{G}(2\omega_1) = 0.48$, $\hat{G}(\omega_L) = 1.00$, $V_1 = V_2 = 1$ V]. This value approximately agrees with the experimentally measured value. The result shows that the detection sensitivity of A_2 is considerably lower than that of A_L. This is consistent with the results obtained in 1 mM NaCl solution [Fig. 3(a)].

2. Potential distribution measurements

Figure 5(b) shows a topographic image of the nanoparticles deposited on the HOPG surface. The image shows several bright spots corresponding to the nanoparticles. Figures 5(c)–5(e) show A_1, A_2, and A_L images simultaneously obtained with the topographic image. From the A_1 and A_2 images, we calculated a potential image in SF mode [Fig. 5(f)]. Similarly, we calculated a potential image from A_1 and A_L images in DF mode [Fig. 5(g)].

While the potential image obtained in DF mode shows clear contrast between the nanoparticles and substrate, but that obtained in SF mode shows no contrast. The difference is also confirmed in the potential profiles measured at the same position of the images. The potential profile [Fig. 5(i)] measured along line C-D in Fig. 5(g) (DF mode) shows that potential of nanoparticles is ~30 mV lower than that of the HOPG substrate. In contrast, the potential profile [Fig. 5(h)] measured along line A-B in Fig. 5(f) (SF mode) shows no difference between nanoparticles and HOPG substrate due to the large noise. These results demonstrate that DF mode enables to operate OL-EPM in a relatively strong electrolyte solution.

We also found that the SNR of the potential measurement in 10 mM solution is lower than that in 1 mM solution. For SF mode, the potential image obtained in 10 mM solution shows no contrast between the nanoparticles and substrate due to the large noise. For DF mode, the potential profile obtained in 10 mM solution [Fig. 5(i)] shows larger noise than that obtained in 1 mM solution [Fig. 3(i)].

These results can be explained as follows. In 1 mM solution, the bias modulation frequencies (600 and 630 kHz) are much higher than f_c (= 50 kHz). In 10 mM solution, however, the modulation frequencies (650 and 680 kHz) are relatively

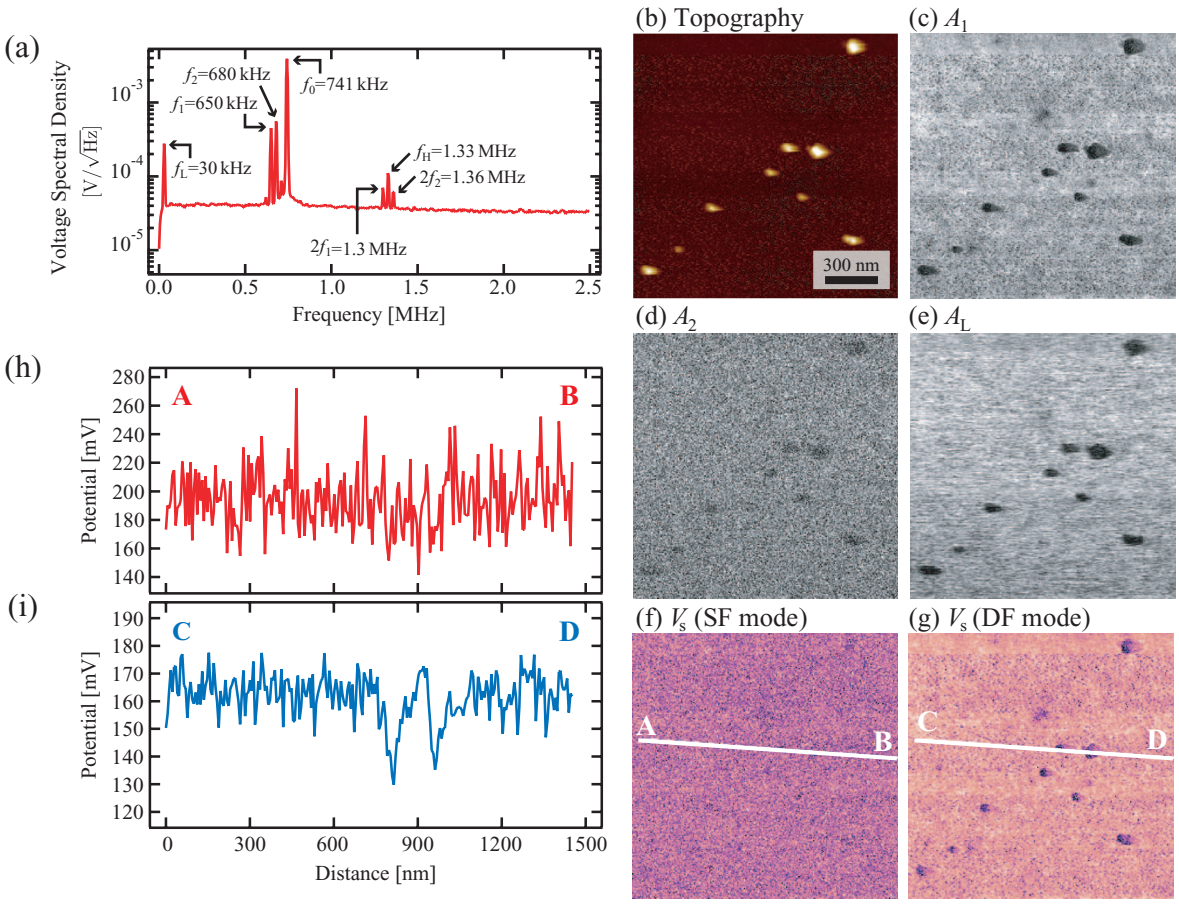

FIG. 5. (a) Voltage spectral density distribution measured in 1 mM NaCl solution on the HOPG surface. (b) Topographic, (c) A_1, (d) A_2, (e) A_L, (f) potenital (SF mode), and (g) potential (DF mode) images of the nanoparticles on the HOPG surface obtained in 10 mM NaCl solution (scan size: 1.5 μm × 1.5 μm, $f_0 = 740.6$ kHz, $Q = 9.6$, $k = 22.5$ N/m, $A = 0.6$ nm, $\Delta f = -450$ Hz, $f_1 = 650$ kHz, $f_2 = 680$ kHz, $V_1 = V_2 = 1$ V). Potential profiles measured along (h) line A-B in (f) (SF mode) and (i) line C-D in (g) (DF mode).

close to f_c (= 300 kHz). Thus, the remaining influence of F_{sp} may have deteriorated the SNR of the potential measurements in 10 mM solution. However, the potential profile shown in Fig. 5(i) shows that DF mode OL-EPM allows us to measure potential distribution with ∼10 mV resolution even in such a strong electrolyte solution.

ACKNOWLEDGMENTS

This work was supported by New Energy and Industrial Technology Development Organization (NEDO) (Grant No. 09A22005a).

[1]R. Sennett and J. P. Olivier, Ind. Eng. Chem. **57**, 32 (1965).
[2]H. J. Butt, B. Cappella, and M. Kappl, Surf. Sci. Rep. **59**, 1 (2005).
[3]D. Ebeling, D. van den Ende, and Frieder Mugele, Nanotechnology **22**, 305706 (2011).
[4]M. Nonnenmacher, M. P. O'Boyle, and H. K. Wickramasinghe, Appl. Phys. Lett. **58**, 2921 (1991).
[5]S. Kitamura and M. Iwatsuki, Appl. Phys. Lett. **72**, 3154 (1998).
[6]Y. Rosenwaks, R. Shikler, Th. Glatzel, and S. Sadewasser, Phys. Rev. B **70**, 085320 (2004).
[7]T. Fukuma, K. Umeda, K. Kobayashi, H. Yamada, and K. Matsushige, Jpn. J. Appl. Phys. **41**, 4903 (2002).
[8]C. Leung, H. Kinns, B. W. Hoogenboom, S. Howorka, and P. Mesquida, Nano Lett. **9**, 2769 (2009).
[9]N. Kobayashi, H. Asakawa, and T. Fukuma, Rev. Sci. Instrum. **81**, 123705 (2010).
[10]H. Asakawa, N. Kobayashi, and T. Fukuma, J. Appl. Phys. **110**, 044315 (2011).
[11]C. Hutter, D. Platz, E. A. Tholén, T. H. Hansson, and D. B. Haviland, Phys. Rev. Lett. **104**, 050801 (2010).
[12]D. Martinez-Martin, E. T. Herruzo, C. Dietz, J. Gomez-Herrero, and R. Garcia, Phys. Rev. Lett. **106**, 198101 (2011).
[13]T. Fukuma, M. Kimura, K. Kobayashi, K. Matsushige, and H. Yamada, Rev. Sci. Instrum. **76**, 053704 (2005).
[14]T. Fukuma and S. P. Jarvis, Rev. Sci. Instrum. **77**, 043701 (2006).
[15]T. Fukuma, Rev. Sci. Instrum. **80**, 023707 (2009).
[16]C. C. Williams, Y. Martin, and H. K. Wickramasinghe, J. Appl. Phys. **61**, 4723 (1987).
[17]D. Horne, T. R. Albrecht, P. Grutter, and D. Rugar, J. Appl. Phys. **69**, 668 (1991).
[18]J. I. Kilpatrick, T. Fukuma, and S. P. Jarvis, Rev. Sci. Instrum. **77**, 123703 (2006).
[19]S. Ishizaki, N. Umeda, and H. Uwai, J. Vac. Sci. Technol. B **9**, 1318 (1991).
[20]K. Umeda, N. Oyabu, K. Kobayashi, K. Matsushige, and H. Yamada, Appl. Phys. Express **3**, 065205 (2010).